JOC The Journal of Organic Chemistry
Cite This: J. Org. Chem. 2019, 84, 817−830
Article
pubs.acs.org/joc

Origin of the Preferential Formation of Helicenes in Mallory Photocyclizations. Temperature as a Tool to Influence Reaction Regiochemistry

J. Weber and E. L. Clennan*

Department of Chemistry, University of Wyoming, Laramie, Wyoming 82071, United States

Supporting Information

ABSTRACT: The regiochemistry of four bis-Mallory photocyclization substrates has been examined from experimental and computational perspectives. Formation of all three possible regioisomers was only observed in the reaction of one of the substrates. In the other three substrates, only the two C_2-symmetric products, but not the C_1 product, were formed. In the three reactions that only formed two products, the photocyclization temperature could be used to select for exclusive formation of one or the other regioisomer. The use of temperature to select between two regioisomers also worked in the photocyclization of the substrate that formed three products. However, no temperature was located for exclusive formation of the third component, one of the C_2-symmetric products, which always formed alongside either one or both of its regioisomers. B3LYP/6-311+G(2d,p) calculations were used to determine the energies of all of the dihydrophenanthrene (DHP), tetrahydrophenanthrene (THP), and mono-Mallory photocyclization intermediates. The oscillator strengths of the DHP precursors to the helicene products were a factor of 4.8−9.2 smaller than those of competitively formed DHPs. This observation suggests that establishment of a photostationary state is responsible for the preferential formation of helicenes that has been observed as a unique and useful feature of many Mallory photocyclizations.

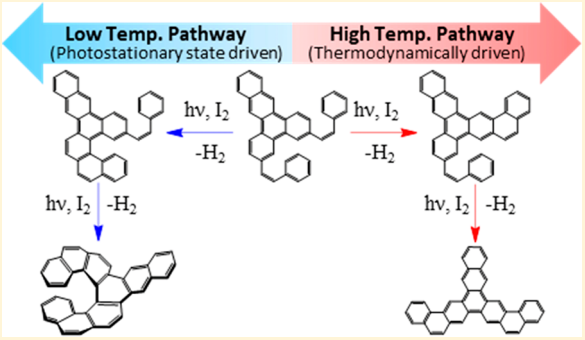

INTRODUCTION

The Mallory photocyclization (Scheme 1) was first observed in 1934 and provided, at the time, an unknown byproduct during the photochemically initiated *cis*−*trans* isomerization of stilbene, **1t** ⇆ **1c**.[1] This byproduct was subsequently identified by Parker and Spoerri[2] in 1950 as phenanthrene. This reaction, although studied sporadically, was more or less dormant until Mallory and co-workers[3] reported in 1962 its development into a preparatively useful oxidative photocyclization by the use of I_2, rather than O_2, as the oxidant (Scheme 1). The key step in the mechanism of the Mallory photocyclization is the widely recognized formation of a *trans*-dihydrophenanthrene (DHP) intermediate[4−7] by an orbital symmetry allowed conrotatory electrocyclic closure (Scheme 1). This skeletal rearrangement in many diaryl-ethylenes is photochromic and consequently has been utilized in the construction of a large number of photoswitching devices.[8] The dihydrophenanthrene, DHP, however, in the Mallory photocyclization is an intermediate, not an end-product, that is subsequently converted to the phenanthrene end-product by abstraction of hydrogen and formation of HI.

Scheme 1. Mechanism for the Mallory Photocyclization of *trans*-Stibene

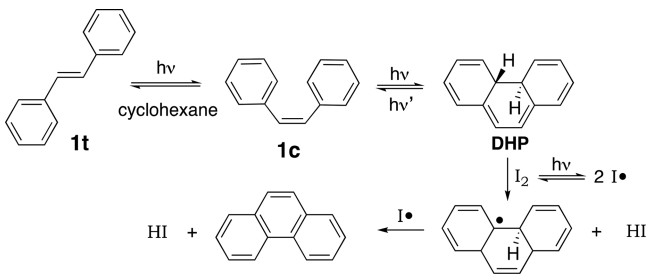

A Mallory photocyclization was used during the first synthesis of [7]helicene[9] and opened the door for decades of study of these fascinating polycyclic aromatic hydrocarbons (PAHs).[10−13] In addition, the importance of the Mallory photocyclization has subsequently been amply demonstrated by the publication of several reviews,[14−19] by the development of useful modifications,[20−26] and most recently by its use in the construction of carbon nanomaterials.[27] The sentence that appears in the elegant review of Morin, Daigel, and Desroche[27]—"The photochemical dehydrogenation, or Mallory reaction, is probably the most widely spread photochemical method for the preparation of carbon nanomaterials and PAHs."—is not hyperbole, and given the seemingly endless applications of PAHs (polycyclic aromatic hydro-

Received: October 16, 2018
Published: December 12, 2018

DOI: 10.1021/acs.joc.8b02671
J. Org. Chem. 2019, 84, 817−830

carbons), it underscores the value of further studies to understand the intimate details of this important reaction.

The mechanistic details of the photochemical interconversion of the *cis*-stilbene, **1c**, to the dihydrophenanthrene, DHP (Scheme 1), step of the Mallory photocyclization have been extensively examined from both experimental[28−30] and theoretical[31−34] perspectives. A two-dimensional slice through the currently accepted potential energy surfaces (PESs) for this reaction step is depicted in Figure 1. Upon irradiation of either

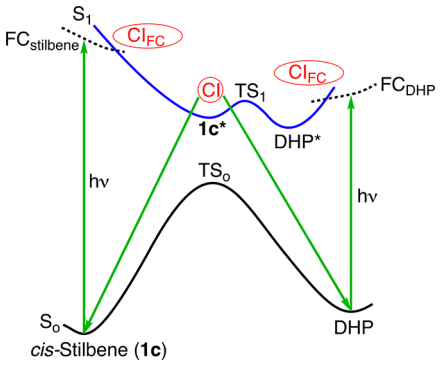

Figure 1. Potential energy surfaces involved in the reversible *cis*-stilbene DHP interconversion.

1c or DHP, an allowed transition to the corresponding Franck−Condon PES, $FC_{stilbene}$ or FC_{DHP}, occurs. Rapid movement on the Franck−Condon PES brings the vibrationally excited state into proximity to a conical intersection, CI_{FC}, where picosecond or sub-picosecond internal conversion to S_1 takes place. Finally, both vibrationally excited states move on the S_1 PES until they reach the critical conical intersection region, CI, where ultrafast deactivation forms either the *cis*-stilbene or the DHP on the S_0 PES. The activation barrier, TS_1 on the S_1 PES, which was predicted theoretically, provides an explanation for both the observed temperature[35] and wavelength[36] dependence of the cycloreversion quantum yield for the DHP.

The detailed understanding of the *cis*-stilbene/DHP interconversion step of the Mallory photocyclization, however, stands in stark contrast to our fundamental lack of understanding, of perhaps the most unusual and distinguishing feature of the Mallory reaction, which is its propensity to form helicenes even when competing photocyclizations to form more thermodynamically stable, sterically less encumbered, planar PAHs are available. This phenomenon is illustrated with the reactions of **2**[37] and **3**,[16] which exclusively produced [6]helicene, **4**, and benzo[*b*]hexahelicene, **5**, without a trace of the alternative photocyclization products (Scheme 2).

Laarhoven and co-workers[38,39] used the Coulson free valence numbers[40] to devise a set of rules to predict the regiochemical outcome of Mallory photocyclizations. These free valence numbers, $\sum F_{rs}^{*}$, are measures of the "residual affinity" for bond formation and are given by $\sqrt{3} - \sum P$ for aromatic carbons, where $\sum P$ is the sum of the bond orders for the three bonds attached to the aromatic carbon in the excited state. According to the Laarhoven rules, when the sum of the free valences of the two carbon atoms that form the new bond in the Mallory reaction is less than 1 (i.e., $\sum F_{rs}^{*} < 1.0$), photocyclization does not occur. This reactivity parameter has been remarkably successful; however, other experimental parameters in addition to the identity of the substrate also influence the extent of regioselectivity, including the concentrations of the oxidant (e.g., I_2, O_2) and substrate, the identity of the solvent, and the temperature.[41] Despite the predictive power of the Laarhoven rules, they do not provide a satisfying rationale or a framework to control the unusual regiochemistry observed in many of these important photocyclizations.

In this manuscript, we describe an experimental and computational study of the bis-Mallory photocyclizations of **6**, **7**, **8**, and **9** (Chart 1) focused on understanding the regioselectivity observed in these reactions. The experimental study reveals that the product regiochemistry in the reactions of **6** and **9** responds very differently to changes in experimental conditions and that the Mallory photocyclizations of **7** and **8** are intermediate in their behavior. The computational results are used to argue that the photostationary state established between competing DHPs plays an important role in these reactions. In addition, in those reactions that produce the helicene as the major product, the photostationary state lies on the side of the DHP precursor to the helicene (DHP′, Chart 1). These results provide valuable insight into Mallory photocyclizations that can be used to design new efficient photocyclization reactions.

Scheme 2. Regioselectivity in Mallory Photocyclizations

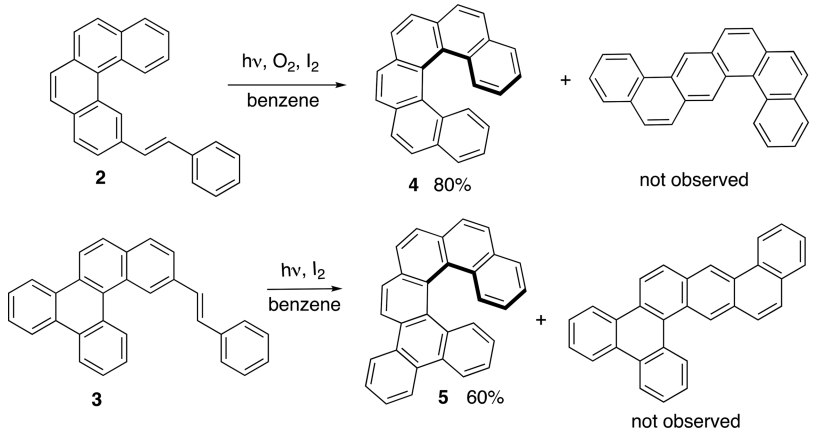

DOI: 10.1021/acs.joc.8b02671
J. Org. Chem. 2019, 84, 817−830

Chart 1

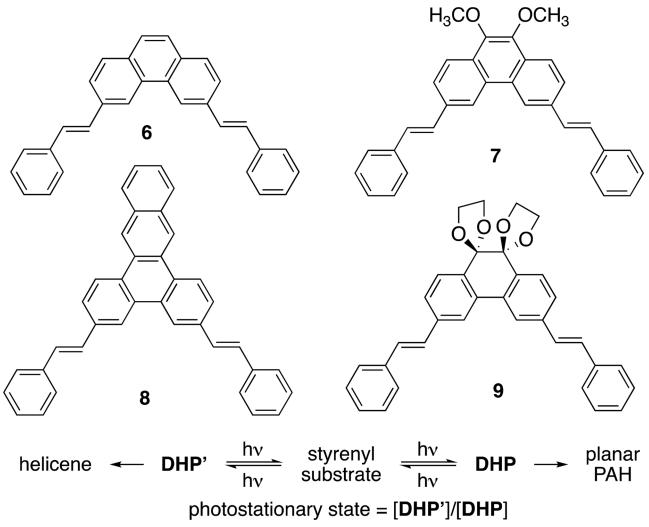

RESULTS

Experimental Studies. Bis-Mallory photocyclization substrates **8** and **9** were synthesized from 3,6-dibromophenanthrenequinone in straightforward two-step procedures, as outlined in Scheme 3. The key steps were the Mizoroki–Heck reactions[42] which had previously been successfully used with 3,6-dibromophenanthrene and 3,6-dibromo-9,10-dimethoxyphenanthrene to make **6** and **7**, respectively.[43] Unfortunately, 3,6-bis-styrenylphenanthrene quinone, despite the fact that it is readily accessible from a Mizoroki–Heck reaction, could not be used in this study. It is completely unreactive under our Mallory photocyclization conditions.

The bis-Mallory photocyclizations were conducted by irradiation (600 W medium pressure mercury vapor lamp) of a 0.5 mM toluene solution of **6**, **7**, **8**, or **9** through the walls of a Pyrex vessel containing 1.1 mM iodine and 25 mM propylene oxide.[20] At room temperature, **9** reacts to give a mixture of all three Mallory photocyclization products, the benzo[*k*]naphtho[1,2-*a*]tetraphene, **10d**, the [7]helicene, **11d**, and the dibenzo[*c*,*m*]pentaphene, **12d** (Chart 2). The benzo[*k*]naphtho[1,2-*a*]tetraphenes, **10a,b,c**, however, were conspicuously absent from room temperature irradiations of **6**, **7**, and **8**. However, oxidation products **15b** and **15c** are formed in approximately 40% yield during bis-Mallory photocyclizations of substrates **7** and **8**, respectively.[44] In addition, diester **16**[45] is also formed in approximately 5% yield in the reactions of **7**. On the other hand, no oxidative cleavage of the styrenyl double bond was observed in any of the phenanthrenyl substrates, **6**–**9**. This suggests that singlet oxygen formed by self-sensitization is involved in these reactions, since the singlet triplet energy gap is 5.4 kcal/mol smaller[46] and the intersystem crossing rate constant[47] to the triplet nearly 3 times larger in the [5]helicene core[48] of **13b,c**, that is oxidatively cleaved to form **15b,c**, than in the phenanthrene core of **6**–**9**, which are oxidatively inert. The formation of diester **16** can be attributed to the well-established enhanced reactivity of singlet oxygen[49,50] with electron rich enol ethers and to the even larger intersystem crossing rate constant of [7]helicene in comparison to that of [5]helicene.[47] The amount of these oxidation products, however, can be substantially reduced by exclusion of oxygen from the reaction mixtures. Products from further complications such as hydrogen shifts in the dihydrophenanthrene, DHP, and *bis*-dihydrophenanthrene, *bis*-DHP, intermediates, which have been observed in other systems, were not detected in the reactions of **6**–**9**.[16]

These reactions were typically conducted overnight and the crude product mixtures analyzed by NMR spectroscopy. Products **11a**, **11b**, and **16** are known, and products **10d**, **11c**, **12c**, **12d**, **15b**, and **15c** were isolated, purified, and fully characterized by ^{1}H and ^{13}C NMR spectroscopy (with the exception of **12c** whose limited solubility precluded collection of its ^{13}C NMR spectrum) and by high-resolution mass spectrometry. Diagnostic peaks in the NMR spectra of these conclusively identified products were then used to identify their homologues (**11d**, **12a**, **12b**, and **12c**) formed in the other Mallory photocyclization reactions. Stacked comparator ^{1}H NMR plots used in this analysis are provided in the Supporting Information for the **11** and **12** homologous series. A diagnostic ddd for proton H_a (Chart 2) showed up in the **11** comparator spectra at approximately 6.4 ppm in all of the [7]helicenes **11a**, **b**, **c**, and **d**. This proton was upfield of all other peaks in the reaction mixtures because it is located in the shielding cone of the terminal ring on the other end of the helicene. The dibenzo[*c*,*m*]pentaphenes, **12**, were also easily identified because Mallory photocyclization conditions (vide infra) are available where these compounds are the major or exclusive product of the reaction. Their most upfield peaks, between 7.6 and 7.7 ppm, are also ddd's and are readily assigned to H_b and H_a. The *cis*- and *trans*-3-strenyl[5]helicenes, **13** and **14**, were identified as fleeting intermediates in the crude reaction mixtures by their characteristic doublet-of-

Scheme 3. Synthesis of Bis-Mallory Photocyclization Substrates 8 and 9

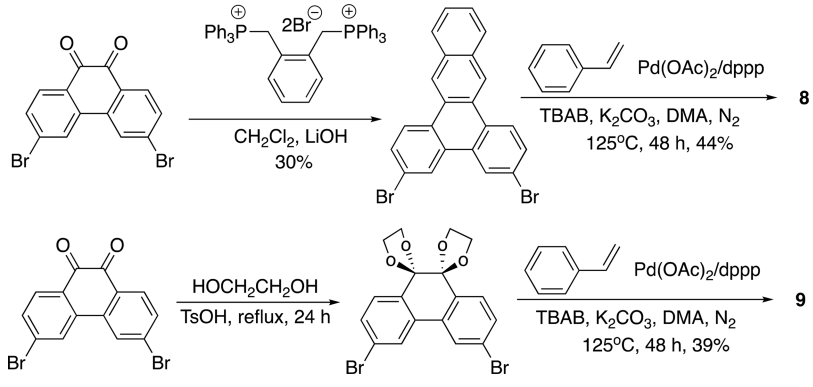

DOI: 10.1021/acs.joc.8b02671
J. Org. Chem. 2019, 84, 817–830

Chart 2

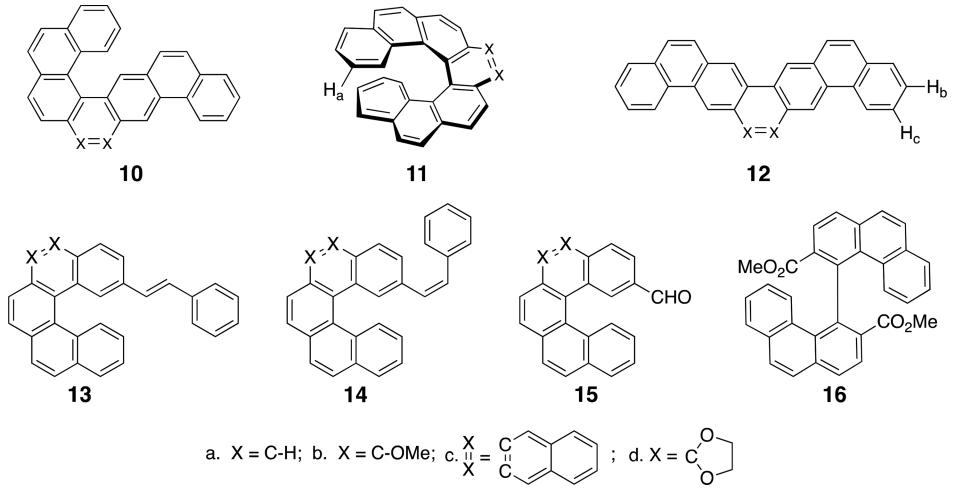

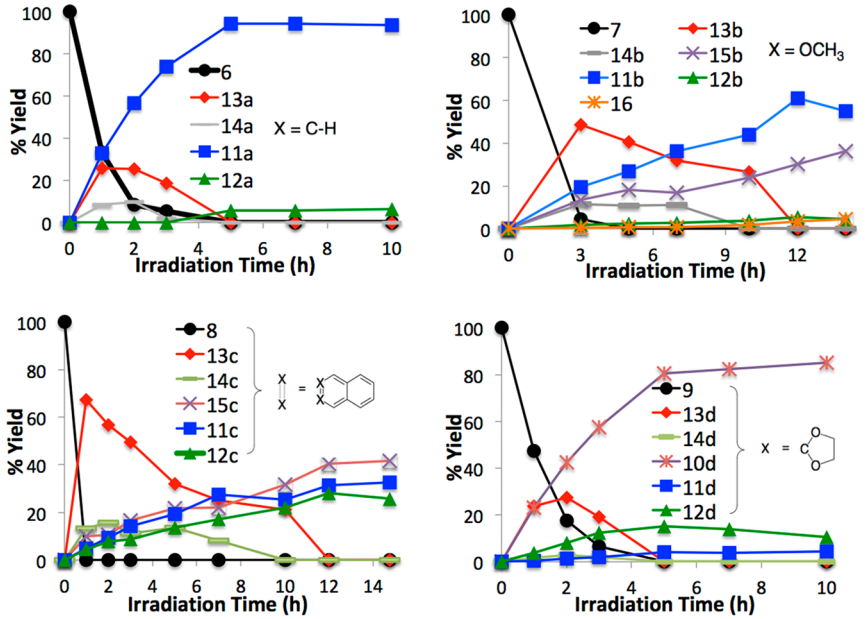

Figure 2. Reaction compositions as a function of time at 40 °C.

doublets for the styrenyl double bond (see the Supporting Information).

The product compositions at approximately 40 °C during Mallory photocyclizations of **6**–**9** as a function of irradiation time are given in Figure 2. The mono-Mallory products **13** and **14** form rapidly followed by slower formation of the [7]helicenes **11**. In addition, the yields of the [7]helicenes decrease in the order **6** > **7** > **8** > **9**. The photocyclization of **9** (Figure 2) was complete in approximately 5 h in comparison to the 10–12 h of irradiation needed to produce the final products in the reactions of **6**, **7**, and **8**. The photocyclization of **9** also produced **10d** under these conditions as the dominant product in approximately 85% yield. In contrast, **10a,b,c** were not observed at any point during the photocyclizations of **6**, **7**, or **8**.

The effect of temperature on the Mallory photocyclizations was examined by running each of the reactions in a pyrex vessel submerged in an appropriate temperature-controlled bath. The products were then analyzed by NMR spectroscopy and their relative yields plotted versus temperature, as depicted in Figure 3. The [7]helicenes, **11a**, **11b**, and **11c**, were the exclusive products in the reactions of **6**, **7**, and **8** at low temperatures (<0 °C). On the other hand, the [7]helicene, **11d**, is observed, but its % yield peaks at approximately 0 °C and never becomes the major product at any temperature between −30 and +150 °C. In all four Mallory photocyclizations, the thermodynamically most stable product (vide infra), the planar dibenzo[*c*,*m*]pentaphene, **12**, is the dominant product at high temperature.

Computational Studies. The mechanisms of the bis-Mallory photocyclizations of **6**–**9** are considerably more complex than the simple photocyclization of *cis*-stilbene shown in Scheme 1. The bis-Mallory substrates undergo two photocyclizations, and each photocyclization can occur at two different sites on the phenanthrene core to give two different DHPs. This leads to 11 different possible closed shell intermediates on these very complicated reaction surfaces in addition to the three possible products, **10**, **11**, and **12**. The structures of all of the potential intermediates are depicted in Chart 3.

DOI: 10.1021/acs.joc.8b02671
J. Org. Chem. 2019, 84, 817–830

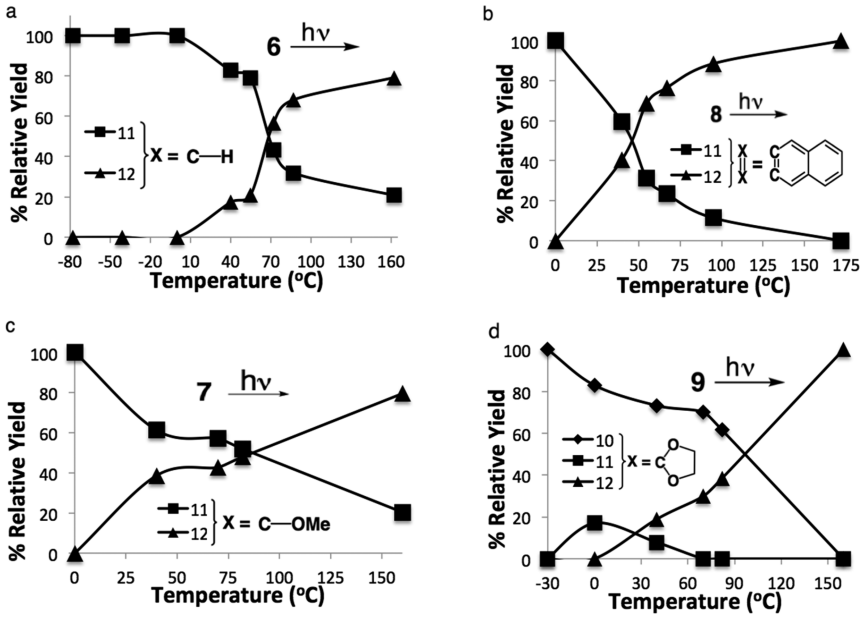

Figure 3. Relative product composition as a function of temperature for the Mallory photocyclizations of **6**, **7**, **8**, and **9**. All reactions were run under an atmosphere of air; however, the oxygenated products are not included in the plots.

Chart 3. Potential Intermediates in the Mallory Bis-Photocyclization of 6

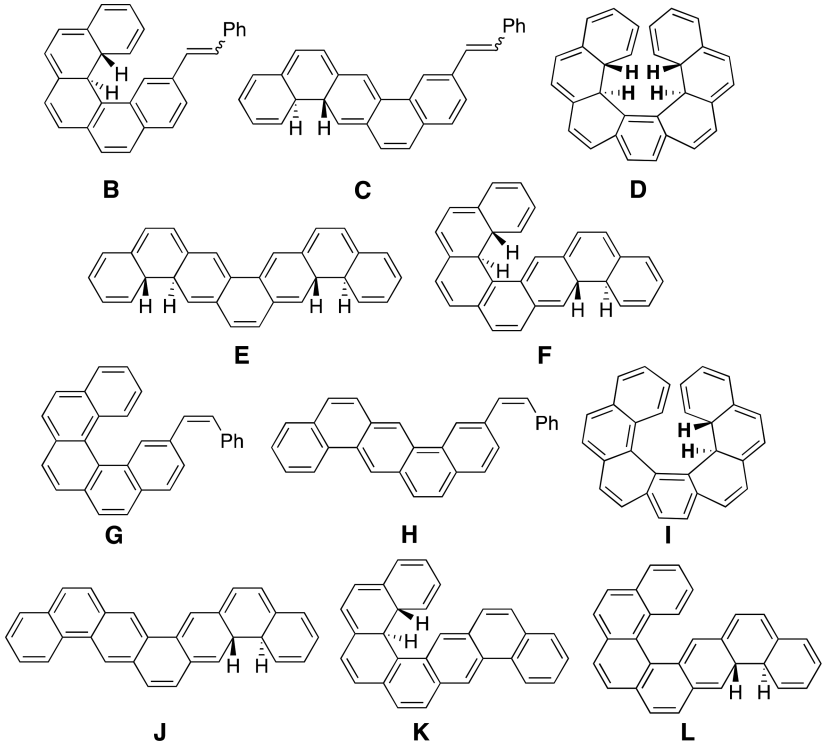

In order to facilitate the consideration of the computational results and the upcoming consideration of potential mechanisms in the Discussion section of the manuscript, these intermediates are organized using the interconversion diagram shown in Scheme 4. However, it is important to recognize that this complicated interconversion diagram is itself a simplification of the actual potential energy surface. Both diastereomers of the DHP regioisomers depicted in Chart 3, which are generated by competing clockwise and counterclockwise ring closures, are not explicitly included in the interconversion diagram. This is not a serious omission. A single diastereomer thermodynamically dominates in most cases (Table 1), but even in those cases where two stereoisomers might be simultaneously present (e.g., $\mathbf{E}_{tct}$ and $\mathbf{E}_{ttt}$ in Table 1; see the Supporting Information for detailed structural information), it will not change the mechanistic conclusions discussed below. Consequently, all of the tables in this manuscript, except Table 1, contain only those values calculated using the thermodynamic data for the most stable diastereomer of each of the DHP regioisomers shown in Chart 3.

DOI: 10.1021/acs.joc.8b02671
J. Org. Chem. 2019, 84, 817−830

Scheme 4. Interconversion Diagram for Intermediates in the Bis-Mallory Photocyclizations of 6, 7, 8, and 9[a]

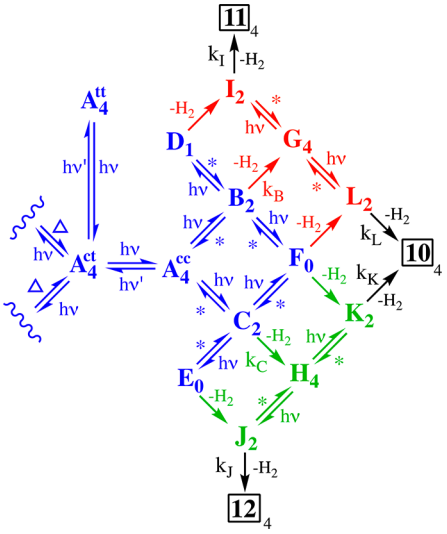

[a]*, *hν* or heat; cc, *cis*–*cis*; ct, *cis*–*trans*; the subscripts on all numerical and letter compound designations refer to its number of Clar sextets.

Table 1. Relative Free Energies[a] of Bis-Mallory Reaction Stationary Points with Zero Negative Frequencies[a]

	C_XH_{Y+4} (Blue Region)[b] Bis-Mallory Reaction Intermediates[c]			
	6(parent)	**7**(di-MeO)	**8**(naphtho)	**9**(bis-ketal)
A	0	0	0	0
B	49.8	50.7	52.8	52.4
$\mathbf{B_a}$	44.2	44.8	46.0	48.1
C	46.1	45.8	42.8	39.1
$\mathbf{D_{iooi}}$	101.7	102.8	105.5	107.4
$\mathbf{D_{oiio}}$	84.3	85.0	90.6	96.7
$\mathbf{D_{oioi}}$	89.9	90.7	97.0	101.3
$\mathbf{E_{tct}}$	85.9	85.6	84.1	78.7
$\mathbf{E_{ttt}}$	85.2	85.8	83.4	78.1
$\mathbf{F_{tct}}$	93.7	93.9	89.4	85.2
$\mathbf{F_{tcta}}$	97.1	97.5	93.7	88.7
$\mathbf{F_{ttt}}$	99.2	99.4	96.1	90.5
$\mathbf{F_{ttta}}$	92.3	92.1	89.0	85.5
	C_XH_{Y+2} (Red/Green Region)[b] Bis-Mallory Reaction Intermediates[c]			
	6(parent)	**7**(di-MeO)	**8**(naphtho)	**9**(bis-ketal)
G	13.4	13.2	13.7	12.4
H	0	0	0	0
I	60.9	61.7	63.7	63.4
$\mathbf{I_a}$	57.4	58.2	60.8	62.2
J	45.0	44.5	42.9	39.5
K	50.4	51.2	53.2	52.0
$\mathbf{K_a}$	44.7	45.0	46.4	47.8
L	61.1	61.1	57.8	52.0
$\mathbf{L_a}$	58.0	58.0	55.3	50.6
	C_XH_Y (Black)[b] Final Reaction Products[c]			
10	13.2	13.7	13.3	11.9
11	24.2	24.4	25.5	23.4
12	0	0	0	0

[a]B3LYP/6-311+G(2d,p) sum of electronic and thermal free energies in kcal/mol. [b]See Scheme 4 for region colors. [c]*X* = number of carbons in **6**–**9**; *Y* = number of hydrogens in the final reaction products, **10**–**12**, of bis-Mallory photocyclization/oxidation of **6**–**9**.

The **A**'s in the interconversion diagram represent the *cis*–*cis* (cc), *cis*–*trans* (ct), and *trans*–*trans* (tt) isomers of the bis-styrenyl starting materials, **6**–**9**, and the subscripts represent the total number of Clar sextets[51] (i.e., the number of six-membered rings with a localized aromatic 6*π* cyclic array of electrons). The remaining letters (see Chart 3 and Scheme 4) represent either dihydrophenanthrenes, **B**, **C**, **I**, **J**, **K**, and **L**, each with 2 Clar sextets, *bis*-dihydrophenanthrenes, **D**, **E**, and **F**, with 1, 0, and 0 Clar sextets, respectively, or mono-Mallory photocyclized intermediates, **G** and **H**, containing 4 Clar sextets. To the left, emanating from $\mathbf{A^{ct}}$ is an identical interconversion diagram differing only from the one on the right by the *trans*-configuration of the styrenyl double bond in intermediates **B**, **C**, **G**, and **H**. The mechanistic conclusions that can be deduced from either wing of the interconversion diagram are identical, so we will use the expanded right-hand wing for the remaining discussion. Intermediates in different colored regions of the diagram are not interconvertible, either thermally or photochemically, because it would require reversible loss of H_2, which is highly improbable. The *'s in the diagram are for microscopic steps that can occur either thermally by a stepwise process or concertedly by a controtatory photochemically allowed process.

DFT based methods with large basis sets have been shown to perform well in thermochemical studies of large polyaromatic hydrocarbons and in studies of delocalized radicals.[52] Consequently, we used the B3LYP/6-311+G(2d,p) computational method to optimize and determine the energies of all of the diastereomers for the regioisomeric intermediates located on the right-hand side of Scheme 4, including the products **10**, **11**, and **12**. The energies are given in Table 1, and the optimized geometries are provided in the Supporting Information.

The stabilities of the $C_{30}H_{22}$ isomers (for **6**) in the blue region and the $C_{30}H_{20}$ isomers in the green/red regions of Scheme 4 decrease with the decreasing number of Clar sextets (blue, $\mathbf{A_4^{cc}} > \mathbf{B_2} \cong \mathbf{C_2} > \mathbf{E_0} \cong \mathbf{F_0}$; green/red, $\mathbf{H_4} \cong \mathbf{G_4} > \mathbf{I_2} \cong \mathbf{J_2} \cong \mathbf{K_2} \cong \mathbf{L_2}$). Superimposed on these primarily aromaticity driven stability sequences, there is also a strain/steric contribution. In the reactions of **6** and **7**, this internal strain raises the energy of the most stable isomer of the tetrahydro[7]helicene **D** with one Clar sextet above that of both **E** and **F** with zero Clar sextets. In the reactions of all of the bis-Mallory substrates, **6**–**9**, the embedded [5]helical structure in **F** raises its energy by 6 or more kcal/mol above that of **E**, despite the fact that both contain the same number of Clar sextets (zero). The internal strain energy imparted by the helical architecture, and the greater strain imparted by the [7]helical architecture relative to the [5]helical architecture, is also expressed in the relative energies of the final bis-Mallory products (**11** > **10** > **12**) all of which can be drawn with 4 Clar sextets (Table 1).

The dihydrophenanthrenes, **B** and **C**, are key intermediates in the blue region (Scheme 4) of the bis-Mallory photocyclizations of **6**–**9**. The most stable isomers of the *bis*-dihydrophenanthrenes, **D**, **E**, and **F** (Table 1), formed in the blue region are approximately 42.6 ± 6.0, 36.6 ± 6.6, and 43.2 ± 5.8 kcal/mol higher in energy than the least stable dihydrophenanthrene and are unlikely to be involved in the reactions. The B3LYP/6-311+G(2d,p) optimized structures of **B** and **C** formed in the photocyclization of **6** are shown in Scheme 5 and have the *trans*-configuration of the hydrogens at the dihydrophenanthrene ring closure junctions, as dictated by

DOI: 10.1021/acs.joc.8b02671
J. Org. Chem. 2019, 84, 817–830

Scheme 5. Structures of the Dihydrophenanthrene Intermediates B and C Formed in the Bis-Mallory Photocyclization of 6

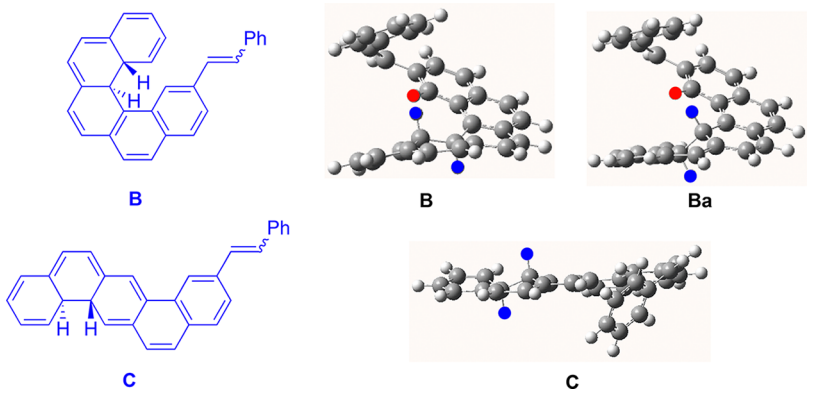

Scheme 6. Structures of the Dihydrophenanthrene Intermediates I, L, J, and K Formed in the Bis-Mallory Photocyclization of 6

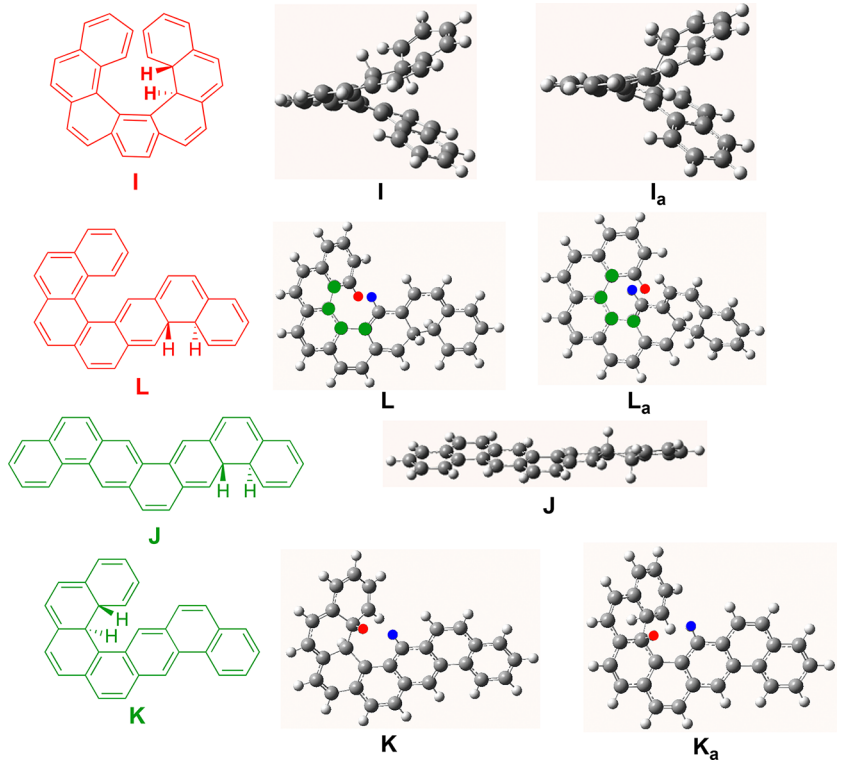

the allowed conrotatory closure. The two conrotatory closures in **B** lead to diastereomers **B** and $\mathbf{B_a}$. Diastereomer **B**(PRR/MSS configuration) is 5.6 kcal/mol less stable than diastereomer $\mathbf{B_a}$ (PSS/MRR configuration) as a result of the 0.36 Å closer approach (1.765 Å vs 2.128 Å) of the blue and red hydrogens (Scheme 5). The two conrotatory closures to form the **C** intermediates are very close in energy at the B3LYP/6-31G(d) computational level ($\Delta\Delta G^{\circ}$(RB3LYP) = 0.4 kcal/mol), so only the most stable diastereomer was optimized at the higher B3LYP/6-311+G(2d,p) computation level and included in Table 1 and Scheme 5.

The key dihydrophenanthrene intermediates in the red and green regions (Scheme 4) of the interconversion diagram, **I**, **J**, **K**, and **L**, which are formed in the photocyclization of **6**, are shown in Scheme 6. (P)-18a(*S*), 18b(*S*)-dihydro[7]helicene $\mathbf{I_a}$ is 3.5 kcal/mol more stable than its isomer (P)-18a(*R*), 18b(*R*)-dihydro[7]helicene **I**. Isomer $\mathbf{I_a}$ is also likely to form faster because it is formed by photocyclization on the least hindered face of the [5]helicene intermediate, **G**. (P)-Naphtho[1,2,*b*]-14a(*R*), 14b(*R*)-dihydro[5]helicene, **K**, is significantly destabilized, by 5.7 kcal/mol, relative to (P)-naphtho[1,2,*b*]-14a(*S*), 14b(*S*)-dihydro[5]helicene, $\mathbf{K_a}$, by the energetically costly 1.78 Å through space H_1–H_{14a} distance, which is increased to a sterically more tolerable 2.23 Å H_1–H_{14b} closest approach distance in $\mathbf{K_a}$ (H_1 blue atom and $H_{14a,14b}$ red atoms in Scheme 6). (P)-1(*R*), 8a(*S*)-dihydronaphtho[1,2,*b*]-[5]helicene, **L**, is 3.1 kcal/mol less stable than its isomer (P)-1(*S*), 8a(*R*)-dihydronaphtho[1,2,*b*]-[5]helicene, $\mathbf{L_a}$, due in part to the shorter H_1–H_{14} (blue and red atoms in Scheme 6) through space distance (2.60 Å in **L** and 2.82 Å in $\mathbf{L_a}$) and by the increased strain in the helical section of the intermediate as revealed by a 3.1° increase in the C_{14a}–C_{14b}–C_{14c}–C_{14d} internal dihedral angle (green atoms in **L** and $\mathbf{L_a}$ in Scheme 6).

DOI: 10.1021/acs.joc.8b02671
J. Org. Chem. 2019, 84, 817–830

The DHPs shown in Schemes 5 and 6 are subsequently oxidized by stepwise removal of two hydrogen atoms with photochemically generated iodine atoms. Aromatic resonance energy is recovered as a result of the second hydrogen abstraction, and as a result, the first hydrogen abstraction is likely to be the rate-determining step for formation of the fully polyaromatic hydrocarbon product. The initial hydrogen abstraction can occur from the terminal or internal ring of the DHP, leading to two different radicals, the *A** and *B** series, respectively. The relative energies of these radicals generated by hydrogen abstraction from $\mathbf{B_a}$, **C**, $\mathbf{I_a}$, **J**, $\mathbf{K_a}$, and $\mathbf{L_a}$ in the reactions of **6** and **9** are given in Table 2. Hydrogen

Table 2. Relative Energies of Radicals Formed in Mallory Cyclizations of 6 and 9[a,b]

	6		9[c]	
	*A**	*B**	*A**	*B**
$\mathbf{B_a}$	1.0	17.6	5.4	15.1
C	1.4	0	0	2.6
$\mathbf{I_a}$	14.2	28.6	19.8	27.6
J	0.6	0	0	2.83
$\mathbf{K_a}$	1.0	16.4	5.2	15.2
$\mathbf{L_a}$	12.1	12.6	11.3	14.9

[a]Relative B3LPY/6-311+G(2d,p) sum of electronic and thermal free energies in kcal/mol for the radicals generated from the most stable DHP diastereomer (see Table 1). [b]*A** - radical formed by hydrogen abstraction from the terminal ring of DHP; *B** - radical formed by hydrogen abstraction from the internal ring of DHP. [c]Calculated at the B3LYP/6-31G(d) level.

abstraction is prohibitively favored ($\Delta\Delta G^\circ \geq 14.4$ kcal/mol) from the terminal ring to give the *A** series when the DHP is part of the helical domain (i.e., $\mathbf{B_a}$, $\mathbf{I_a}$, and $\mathbf{K_a}$). On the other hand, the energies of the *A** and *B** series radicals, formed by hydrogen abstraction from the DHPs that reside in the acene domain (i.e., **C**, **J**, and $\mathbf{L_a}$), are nearly equal. Formation of the *A** series radicals from the helical embedded DHPs opens up the jaws of the helicene decreasing steric interactions, while formation of the *B** series radicals closes the jaws and increases the intrahelicene steric interactions (Scheme 7). The formation of the *A** series radicals in the helical domain embedded DHPs is also likely kinetically preferred, since the hydrogen on the terminal ring is on the periphery of the helicene while the internal hydrogen is buried in the jaws of the helical cleft (see $\mathbf{B_a}$ in Scheme 5 and the Supporting Information).

The UV−vis spectra of the DHPs were calculated using the TD-DFT/6-311+G(2d,p) computational model. The lowest energy transitions are given in Table 3 along with their oscillator strengths. The DHPs (i.e., $\mathbf{B_a}$ and **C**, $\mathbf{I_a}$ and $\mathbf{L_a}$, and

Table 3. Wavelength Maxima and Oscillator Strengths of Low Energy DHP UV/Vis Absorbances[a]

	λ_{max}[b]	*f*[c]		λ_{max}[b]	*f*[c]
			6		
$\mathbf{B_a}$	683	0.0622	**C**	663	0.3135
$\mathbf{I_a}$	689	0.0628	$\mathbf{L_a}$	704	0.3325
$\mathbf{K_a}$	727	0.0527	**J**	662	0.4857
			7		
$\mathbf{B_a}$	688	0.0619	**C**	670	0.2946
$\mathbf{I_a}$	696	0.0631	$\mathbf{L_a}$	713	0.3154
$\mathbf{K_a}$	732	0.0514	**J**	670	0.4500
			8		
$\mathbf{B_a}$	717	0.0617	**C**	624	0.4144
$\mathbf{I_a}$	730	0.0629	$\mathbf{L_a}$	667	0.4358
$\mathbf{K_a}$	743	0.0683	**J**	630	0.5821
			9		
$\mathbf{B_a}$	713	0.0877	**C**	585	0.4764
$\mathbf{I_a}$	720	0.0888	$\mathbf{L_a}$	601	0.5019
$\mathbf{K_a}$	730	0.1019	**J**	607	0.6746

[a]Calculated at the TD-DFT/6-311+G(2d,p) level in toluene. [b]Wavelength of the lowest energy transition. [c]Oscillator strength.

$\mathbf{K_a}$ and **J**) in the same colored region of Scheme 4 are thermally and photochemically interconvertible and are placed in the same rows of Table 3 for comparison. The HOMO−LUMO determinant in all cases was the ≥99% contributor to the excited-state wave function as determined by taking 2 times the square of the coefficient for the configuration interaction expansion. The absorbance maxima are all between 580 and 750 nm consistent with the transient formation of a colored intermediate noted in many Mallory photocyclizations.[53] For example, the bathochromic absorption maxima for DHPs **17**, **18**, and **19** (Chart 4) are reported at 603, 448, and 530 nm,

Chart 4

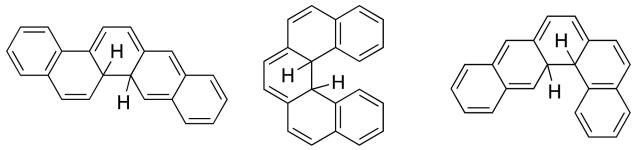

17 **18** **19**

respectively, with extinction coefficients of approximately 10 000−12 000 M^{-1} cm^{-1}.[54] The oscillator strengths (*f*) for the DHPs embedded in helical domains (column 3) were 5 to

Scheme 7. Steric Interactions in $6I_a$ in Comparison to Those Observed in *A and *B** and Series Hydrogen Abstraction Products (Radicals)**

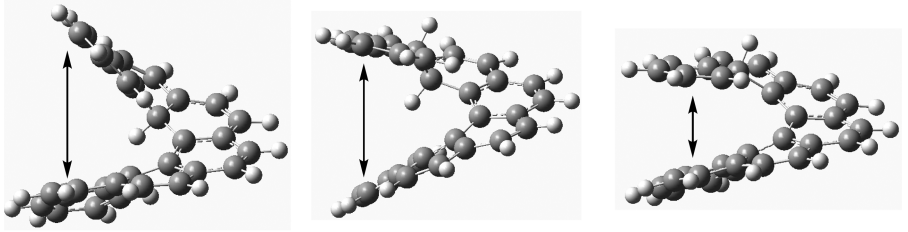

$6I_a$• A* series $6I_a$ $6I_a$• B* series

DOI: 10.1021/acs.joc.8b02671
J. Org. Chem. 2019, 84, 817−830

approximately 9 times smaller than those embedded in acene domains (column 6, Table 3).

DISCUSSION

As evident from examination of the interconversion diagram in Scheme 4, the yields of the three products formed in the bis-Mallory photocyclizations are sensitive functions of the concentrations of the DHPs ([**B**], [**I**], etc.) and of the rate constants for hydrogen abstraction, k_{DHP} (e.g., k_I, k_B, etc.). This is expressed mathematically in eqs 1, 2, and 3. The yield of **11**, for example, is the product of the fraction of the precursor **B** formed in the blue region $\varnothing_B$ and the fraction of **I** formed in the red region $\varnothing_I$. The yield of **10** on the other hand has two terms, since it can be formed in both the green and red regions of Scheme 4.

$$\%\mathbf{10} = [\varnothing_L\varnothing_B + \varnothing_K\varnothing_C] \times 100 \quad (1)$$

$$\%\mathbf{11} = \varnothing_I\varnothing_B = \left(\frac{k_I[I]}{k_I[I] + k_L[L]}\right)\left(\frac{k_B[B]}{k_B[B] + k_C[C]}\right) \times 100 \quad (2)$$

$$\%\mathbf{12} = \varnothing_J\varnothing_C = \left(\frac{k_J[J]}{k_J[J] + k_K[K]}\right)\left(\frac{k_C[C]}{k_B[B] + k_C[C]}\right) \times 100 \quad (3)$$

Several experimental and structural variables can influence the concentrations of the DHPs and the rate constants of hydrogen abstraction, k_{DHP}, whose magnitudes dictate product formation (eqs 1, 2, and 3). These include the following: (1) the position of the photostationary state established between the two competing DHPs, (2) the relative stability of the competing DHPs, (3) the relative stabilities of DHP radicals (A^*) produced during hydrogen abstraction from the competing DHPs, and (4) experimental variables such as reaction temperatures.

(1) The photostationary states established between the two competing DHPs in the mutually inaccessible blue, red, and green regions of Scheme 4 are given by eqs 4a, 4b, and 4c, respectively. These equations are analogous to the equation for the photostationary state reached upon irradiation of *cis*- and *trans*-alkenes,[55] but differ because they are the product of two photostationary equilibria, for example, **L** ⇆ **G** and **G** ⇆ **I** in the red region of Scheme 4 to give eq 4b. The ratio, of the extinction coefficients, $\varepsilon_L/\varepsilon_I$, at the λ_{max} of the HOMO → LUMO absorption peaks for the DHPs shown in Table 3, is proportional to the ratio of oscillator strengths[56] (Table 3) when the band widths are the same. This relationship also implies that the ratio of DHP concentrations will change with changing irradiation wavelength. This is consistent with the observation of Fischer and co-workers[53] who observed a strong wavelength dependence on the ratio of DHP_X/DHP_Y during the Mallory photocyclization of 1,2-di(2-naphthyl)-cyclopentene (Scheme 8).

$$\frac{[B]}{[C]} = \frac{\varepsilon_C}{\varepsilon_B} \cdot \frac{(\phi_{A\to B})(\phi_{C\to A})}{(\phi_{B\to A})(\phi_{A\to C})} \quad \mathbf{4a}$$

$$\frac{[I]}{[L]} = \frac{\varepsilon_L}{\varepsilon_I} \cdot \frac{(\phi_{G\to I})(\phi_{L\to G})}{(\phi_{I\to G})(\phi_{G\to L})} \quad \mathbf{4b}$$

$$\frac{[K]}{[J]} = \frac{\varepsilon_J}{\varepsilon_K} \cdot \frac{(\phi_{H\to K})(\phi_{J\to H})}{(\phi_{K\to H})(\phi_{H\to J})} \quad \mathbf{4c}$$

Scheme 8. DHP Diastereomers Formed during Mallory Photocyclization of 1,2-Di-(2-naphthyl)cyclopentene

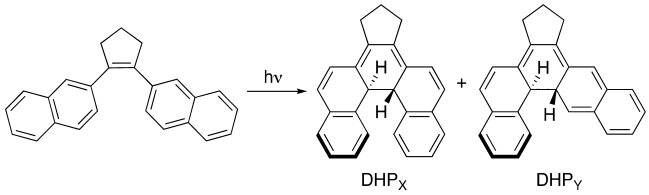

(2) The relative stabilities of the competing DHPs in the blue (**B**$_a$−**C**), red (**I**$_a$−**L**$_a$), and green (**K**$_a$−**J**) regions of the mechanism shown in Scheme 4 are compared in terms of both their free energies in Table 1 and enthalpies in Table 4. This data reveals that the DHPs in the reactions of **6** and **7** that are embedded in the helical domain, **B**$_a$, **I**$_a$, and **K**$_a$, and are the precursors for formation of a helical product, are equal or perhaps slightly more stable than the DHPs embedded in the acene domain, **C**, **L**$_a$, and **J** (columns 2 and 3 in Table 4). On the other hand, Mallory substrates **8** and **9** exhibit the opposite behavior with their acene-embedded DHPs, **C**, **L**$_a$, and **J**, more stable than their helicene-embedded DHPs, **B**$_a$, **I**$_a$, and **K**$_a$. This stability preference for **C**, **L**$_a$, and **J** in **9** is especially large (7.0−10.1 kcal/mol) and essentially precludes all but a trace of **B**$_a$, **I**$_a$, and **K**$_a$ at thermodynamic equilibrium.

(3) The relative stabilities of DHP radicals formed in reactions with the iodine atom/radical can also potentially play an important role in the rates of hydrogen abstraction. The relative stabilities of radicals generated by abstraction of hydrogen from the terminal unsaturated ring of the DHPs (series A^* radicals) are given in Table 2. In the reaction of **6**, the stability differences between radicals formed from competing DHPs, **B**$_a$−**C**, **I**$_a$−**L**$_a$, and **J**−**K**$_a$, are very small, −0.4, +2.1, and −0.4 kcal/mol, respectively. In stark contrast, these energy differences, **B**$_a$−**C**, **I**$_a$−**L**$_a$, and **J**−**K**$_a$, +5.4, +8.5, and −5.2 kcal/mol, respectively, are much larger in the reaction of **9**. These values can be used in conjunction with eq 5 shown in Figure 4 to generate the differences in the enthalpies of reaction for abstraction of the first hydrogen from the competing DHPs with the iodine atom (Table 4, columns 5 and 6). In **6**, these endothermic hydrogen abstractions are energetically more favorable from their acene-embedded DHPs, **C**, **L**$_a$, and **J**, while, in substrate **9**, they are more favorable from their helicene-embedded DHPs (Table 4, columns 6 and 7). In both cases, hydrogen abstraction is enthalpically more favorable from the least stable set of DHPs.

(4) Increasing temperature can (a) enhance the rate of passage over the TS_1 barrier on the Mallory photocyclization S_1 PES (Figure 1), (b) increase the rate of thermal decompositions of the DHPs, and (c) increase the rate of hydrogen abstraction by iodine atom from the DHPs.

DOI: 10.1021/acs.joc.8b02671
J. Org. Chem. 2019, 84, 817−830

Table 4. Differences in Enthalpies and Free Energies of Formation and for Hydrogen Abstraction from DHPs with Iodine Atom[a]

	$\Delta\Delta H_f^\circ$ (**6**)[b]	$\Delta\Delta H_f^\circ$ (**7**)[b]	$\Delta\Delta H_f^\circ$ (**8**)[b]	$\Delta\Delta H_f^\circ$ (**9**)[c]	$\Delta\Delta H_{Rxn}^\circ$ (**6**)[d]	$\Delta\Delta H_{Rxn}^\circ$ (**9**)[d]
($\mathbf{B_a}$–**C**)	−2.6(−1.9)	−1.9(−1.0)	+2.3(+3.2)	+7.8(+8.3)	+1.21(+1.61)	−2.29(−2.89)
($\mathbf{I_a}$–$\mathbf{L_a}$)	−1.2(−0.6)	−0.6(+0.2)	+4.9(+5.5)	+10.1(+11.1)	+2.59(+2.72)	−2.58(−2.64)
($\mathbf{K_a}$–**J**)	−1.0(−0.3)	−0.3(+0.5)	+2.2(+3.5)	+7.0(+7.8)	+0.42(+0.63)	−2.62(−2.59)

[a]$\Delta\Delta G_f^\circ$ in parentheses. [b]In kcal/mol calculated at the B3LYP/6-311+G(2d,p) computational level. [c]In kcal/mol calculated at the B3LYP/6-31G(d) computational level. [d]Calculated using eq 5 shown in Figure 4.

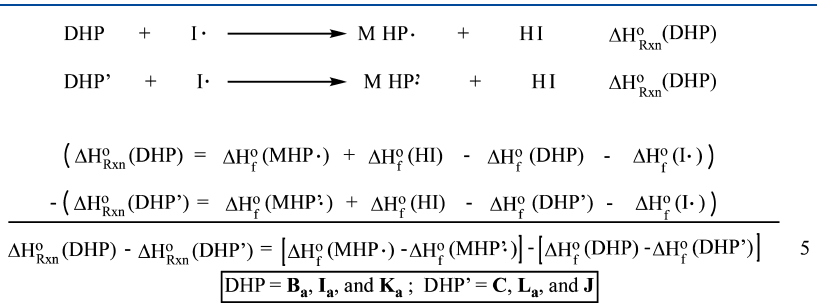

Figure 4. Equation 5 to determine $\Delta\Delta H_{Rxn}^\circ$ for **6** and **9** (Table 4).

(a) Dulić and co-workers[35] have examined the temperature dependence of passage over the TS1 barrier for a series of *cis*-stilbene photochromic switches. The rate of approach to the open/closed photostationary state is temperature independent at temperatures above 0 °C where most Mallory photocyclizations are conducted. At temperatures below 0 °C, the quantum yields (e.g., $\phi_{A\rightarrow B}$, $\phi_{J\rightarrow H}$, etc.) may exhibit small changes as a function of temperature; however, to a large extent, these changes are likely to cancel each other out in the quantum yield ratios (e.g., $[(\phi_{A\rightarrow B})(\phi_{C\rightarrow A})]/[(\phi_{B\rightarrow A})(\phi_{A\rightarrow C})]$, etc.) that are directly proportional to the steady state concentrations of the competing DHPs (eqs 4a, 4b, and 4c). *trans*-Stilbene but not *cis*-stilbene also encounters an activation barrier on the way to the twisted phantom intermediate on its geometric isomerization energy surface, and as a result, competitive fluorescence is observed in solution for the *trans*- but not the *cis*-isomer.[57] This barrier, however, is only 3.5 kcal/mol[58] and, consequently, unlikely to influence the *cis*-/*trans*-stilbene photostationary state at temperatures used for Mallory photocyclizations. It is also worthwhile to note that the **13**/**14** *cis*/*trans* photostationary state is established early on in the bis-Mallory photocyclization PES (Figure 2) and is maintained throughout the reaction.

(b) DHPs have been directly observed, and their thermal decompositions have been monitored.[54] The lifetimes of the DHPs have also been measured, but their accuracy, and what is really being measured, is debatable because of the wide range of processes including oxidation and rearrangements that contribute to their decompositions. Nevertheless, the thermal decompositions of the competing DHP isomers in the blue, red, and green regions of the interconversion diagram (Scheme 4) with the greatest internal energy are expected to be more facile. The concerted thermal conrotatory openings of the DHPs reported here are not allowed; however, their high-energy content (>39 kcal/mol relative to their styrenyl precursor; Table 1) provides a driving force for their homolytic cleavage initiated decompositions to regenerate the Mallory substrates.

(c) In DHPs $\mathbf{B_a}$, $\mathbf{I_a}$, and $\mathbf{K_a}$, the two hydrogens available for abstraction differ in their accessibility to the iodine atom and lead to radicals of very different thermodynamic stabilities (Table 2). In contrast, both hydrogens in DHPs **C**, **J**, and $\mathbf{L_a}$ are equally accessible for abstraction and lead to nearly isoenergetic radicals. Consequently, the rate constants for hydrogen abstraction will increase with increasing temperature more rapidly for DHPs **C**, **J**, and $\mathbf{L_a}$ than for DHPs $\mathbf{B_a}$, $\mathbf{I_a}$, and $\mathbf{K_a}$, since they enjoy an $R\ln 2$ symmetry contribution to the entropy of activation.

Reaction Mechanisms for Mallory Substrates 6, 7, 8, and 9. The bis-Mallory photocyclizations of **6**, **7**, **8**, and **9** are very complex reactions (Scheme 4) and, as discussed above, depend upon a myriad of experimental conditions and substrate structural features that can influence their choice of reaction pathway. Detailed photophysical studies will be required to unravel the precise mechanistic details for each of these bis-Mallory substrates. Nevertheless, it is useful to qualitatively examine how the factors discussed above can influence the reaction pathways and product distributions in these substrates.

*Mallory Photocyclization Substrates **6** and **7**.* At 0 °C and below, Mallory substrates **6** and **7** exclusively produce the helicene products **11a** and **11b**, respectively (Scheme 4). This is consistent with preferential photostationary formations of **B** and **I**, since the ratios $\varepsilon_C/\varepsilon_B$ and $\varepsilon_L/\varepsilon_I$ for **6** and **7**, respectively, are equal to the ratios of the oscillator strengths and the smaller oscillator strength of the DHP precursor to **11a** and **11b** (e.g., $f_C/f_B(\mathbf{6}) = (0.3135/0.0622) = 5.04$ and $f_C/f_B(\mathbf{7}) = (0.2946/0.0619) = 4.76$; Table 3) means that their concentrations build up because they absorb less light. However, in order to attain [B]/[C] and [I][/[L] ratios of 20 or greater (i.e., exclusive detection of **11a** and **11b**), it would also require that $[(\phi_{A\rightarrow B})(\phi_{C\rightarrow A})]/[(\phi_{B\rightarrow A})(\phi_{A\rightarrow C})]$ and $[(\phi_{G\rightarrow I})(\phi_{L\rightarrow G})]/[(\phi_{I\rightarrow G})(\phi_{G\rightarrow L})]$ (see eqs 4a and 4b) have values of approximately 4−5. We argue that values of 4−5 are reasonable and are consistent with the Laarhoven effect that suggests (vide supra) that bonding occurs between carbon atoms where the "residual affinity" for bond formation is the greatest, which in many cases leads to preferential helicene formation. Consequently, the Laarhoven (kinetic) effect in the photocyclizations of **6** and **7** requires the blue quantum yields, $(\phi_{A\rightarrow B})$ and $(\phi_{G\rightarrow I})$ appearing in eqs 4a and 4b, involving formation or extension of a helical structure to be larger than

DOI: 10.1021/acs.joc.8b02671
J. Org. Chem. 2019, 84, 817−830

the red quantum yields, ($\phi_{B\rightarrow A}$) and ($\phi_{I\rightarrow G}$) appearing in eqs 4a and 4b, that involve loss or decrease of helical structure. This observation, coupled with the fact that the black quantum yields for the photoreversible formation of DHPs, that do not involve formation, extension, loss, or decrease in helical structure, are more comparable in magnitude, ($\phi_{C\rightarrow A}$) ≈ ($\phi_{A\rightarrow C}$) and ($\phi_{L\rightarrow G}$) ≈ ($\phi_{G\rightarrow L}$), support our contention that values of 4−5 for the ratio of quantum yields in eqs 4a and 4b are reasonable. As the temperature is raised, the photostationary state favoring helicene formation is not established; instead, for example, in the case of **6**, the 3.65 and 1.94 kcal/mol (Table 4) energetically preferred hydrogen abstractions from DHPs **C** and **J**, respectively, serve to shift the **B** ⇆ **C** and **K** ⇆ **J** equilibrium toward these more stable DHPs and ultimately produce the high temperature products **12a** and **12b**.

Mallory Photocyclization Substrate ***8***. At 0 °C, the helicene, **11c**, is the exclusive product of the Mallory photocyclization of **8**. However, the concentration of the dibenzopentaphene product, **12c**, becomes approximately equal to the concentration of **11c** at 30−40 °C at lower temperatures than those observed for **6** and **7** (Figure 3). This is consistent with the observation that DHPs, **C** and **J**, on the way to **12c** are 3.2 and 3.5 kcal/mol more stable than their competitively formed DHPs $\mathbf{B}_a$ and $\mathbf{K}_a$, respectively (Tables 1 and 4). Consequently, the rates of hydrogen abstraction, k_C[**C**][I•] and k_J[**J**][I•], because of the higher concentrations of **C** and **J**, can more effectively compete with establishment of the photostationary state and enhance the amount of **12c** formed in the photocyclization. In comparison, in the reactions of **6** and **7**, DHPs, **C** and **J**, on the way to **12a** and **12b**, respectively, are far less stable relative to their competitively formed DHPs $\mathbf{B}_a$ and $\mathbf{K}_a$ (Tables 1 and 4). As a consequence, formation of **12a** and **12b** does not compete as effectively with formation of **11a** and **11b** and a higher temperature is required for their concentrations to become equal (i.e., [**12a**] = [**11a**] and [**12b**] = [**11b**]).

Mallory Photocyclization Substrate ***9***. Photocyclization of **9** at −30 °C unexpectedly generated benzo[*k*]naphtho[1,2-*a*]tetraphene, **10d**, as the only product (Figure 3d). In contrast to the other two possible regioisomers, **11d** and **12d**, it can form in either the red or green regions of the interconversion diagram shown in Scheme 4. However, irradiation of **9** is anticipated to predominantly generate DHP **C** because it is 9 kcal/mol more stable than $\mathbf{B}_a$ (Table 1). Nevertheless, at −30 °C, hydrogen abstraction from DHP **C** does not enjoy as large a symmetry advantage ($T\Delta S = T \ln 2$) as it would have at higher temperatures, and its lifetime is extended sufficiently to allow formation of the photostationary state and DHP $\mathbf{B}_a$. Hydrogen abstraction to form **G** followed by exclusive photocyclization to form $\mathbf{L}_a$, driven by its very large thermodynamic stability (11.6 kcal/mol) relative to $\mathbf{I}_a$ (Table 1), subsequently generates the observed product, **10d**. (Note: For comparison, $\mathbf{I}_a$ and $\mathbf{L}_a$ formed in the photocyclizations of **6** and **7** (Table 1) are nearly identical in energy.) This scenario is supported by the fact that at slightly higher temperatures the less stable $\mathbf{I}_a$ is increasingly populated and **11d** forms but then decreases (Figure 3) as it succumbs to the thermodynamic stabilities of DHPs **C** and **J** on the way to the thermodynamically most stable regioisomer **12d**.

CONCLUSIONS

Mallory substrates, **6**, **7**, and **8**, react at low temperatures to exclusively produce their helicene products, **11a**, **11b**, and **11c**, despite the fact that their regioisomers, **10a**, **10b**, and **10c**, that can form competitively are 11.0, 10.7, and 12.2 kcal/mol more stable. This unusual, and synthetically useful, observation can be attributed to three effects: (1) the energies of the DHP precursors to these two sets of regioisomers are much closer in energy (≤5.5 kcal/mol) than the 10.7−12.2 kcal/mol separating the energies of the final regioisomeric products; (2) the extinction coefficients of the DHP precursors to the helicenes are smaller than the extinction coefficients of DHP precursors to their regioisomers by a factor of 4.8−9.2; and (3) at low temperatures thermal decompositions of intermediates are suppressed. Consequently, these effects allow attainment of the photostationary state while suppressing thermal decomposition of the DHPs and simultaneously bias the photostationary state toward population of the DHP precursor to the helicene product. This provides a satisfying and compelling rationale for what many feel is the most bizarre feature of Mallory photocyclization reactions, the preferential formation of the thermodynamically least stable helicene regioisomer.

Unparalleled control over product regiochemistry in Mallory photocyclizations is now available by rationale design of substrates to influence dihydrophenanthrene (DHP) intermediate stability and the magnitudes of their extinction coefficients. These structural controls coupled with the ability to use temperature to influence the approach to the DHP photostationary state enhance the utility of one of the most widely used photochemical methods for formation of polycyclic aromatic hydrocarbons.

EXPERIMENTAL SECTION

3,6-Dibromobenzo[*f*]tetraphene. A CH_2Cl_2 (32 mL) suspension of 3,6-dibromophenanthrenequinone (0.25g, 0.68 mmol) and *o*-xylylenebis(triphenylphosphonium bromide) (0.625 g, 0.79 mmol) was stirred until homogeneous. The stir bar was removed, and 15 mL of freshly prepared LiOH solution (3.36 M, 0.35 g of Li metal in 15 mL of water) was added. The two-phase mixture was sonicated for 80 min. The reaction product was extracted with CH_2Cl_2 and washed with water. The crude product was purified by silica gel chromatography (toluene) and was finally recrystallized from the eluent to give (90 mg, 30%) of 2,13-dibromobenzo[*b*]triphenylene as colorless needles. ^{1}H NMR (400 MHz, $CDCl_3$, δ): 7.58−7.60 (m, 2H), 7.76 (dd, J = 1.9 Hz, 8.7 Hz, 2H), 8.05−8.07 (m, 2H), 8.55 (d, J = 1.9 Hz, 2H), 8.58 (d, J = 8.8 Hz, 2H), 8.97 (s, 2H). ^{13}C{^{1}H} NMR (100 MHz, $CDCl_3$, δ): 122.4 (2C), 122.4 (2C), 125.7 (2C), 126.6 (2C), 126.8 (2C), 127.6 (2C), 128.3 (2C), 129.5 (2C), 130.8 (2C), 131.3 (2C), 132.6 (2C). See the Supporting Information for the details of the X-ray structure of 2,13-dibrombenzo[b]triphenylene.

3,6-Di((*E*)-styryl)benzo[*f*]tetraphene (8). A mixture of 2,13-dibromobenzo[*b*]triphenylene (66.5 mg, 0.14 mmol), tetra-*n*-butylammonium bromide (108 mg, 0.34 mmol), and K_2CO_3 (84.4 mg, 0.61 mmol) in 4 mL of DMA was stirred and heated to 120 °C under nitrogen. When 60 °C was reached, the reaction mixture was charged with styrene (47.5 mg, 0.46 mmol). When 90 °C was reached, a prepared palladium catalyst solution was added dropwise ($Pd(OAc)_2$ (0.7 mg, 3 μmol), 1,3-bis(diphenylphosphino)propane (1.9 mg, 4.6 μmol) in 4 mL of DMA). This reaction was then stirred at 120 °C for 48 h and then allowed to cool to room temperature and transferred to a separatory funnel along with 25 mL of 6 N HCl. The reaction product was extracted with CH_2Cl_2 and washed with 6 N HCl and water. Removal of the solvent produced an off-white solid in nearly quantitative yield that was used in the next step without purification. An analytically pure sample for characterization was obtained by washing with acetone to give a white solid. (30 mg, 44%)

DOI: 10.1021/acs.joc.8b02671
J. Org. Chem. 2019, 84, 817−830

^{1}H NMR (400 MHz, $CDCl_3$, δ): 7.32−7.48 (m, 10H), 7.58−7.61 (m, 2H), 7.68 (d, J = 8.1 Hz, 4H), 7.93 (dd, J = 1.4 Hz, 8.5 Hz, 2H), 8.11−8.13 (m, 2H), 8.71 (d, J = 1.5 Hz, 2H), 8.79 (d, J = 8.6 Hz, 2H), 9.09 (s, 2H). ^{13}C{^{1}H} NMR (100 MHz, $CDCl_3$, δ): 122.2 (2C), 122.2 (2C), 122.3 (2C), 124.3 (2C), 125.2 (2C), 126.2 (2C), 126.7 (4C), 127.9 (2C), 128.2 (2C), 128.4 (2C), 128.8 (4C), 128.8 (2C), 128.9 (2C), 129.6 (2C), 129.9 (2C), 132.4 (2C), 136.7 (2C). HRMS (MALDI-TOF) m/z calculated for $C_{38}H_{27}$ [M + H]$^+$, 483.2113; found, 483.2144.

3,6-Di((*E*)-styryl)-9,10-bis-ethyleneketalphenanthrene (9). A mixture of 3,6-dibromo-9,10-bis-ethyleneketalphenanthrene (280 mg, 0.62 mmol), tetra-*n*-butylammonium bromide (480 mg, 1.49 mmol), and K_2CO_3 (103 mg, 0.74 mmol) in 6 mL of DMA was stirred and heated up to 120 °C under nitrogen. When 60 °C was reached, the reaction mixture was charged with styrene (193 mg, 1.86 mmol). When 90 °C was reached, a prepared palladium catalyst solution was added dropwise ($Pd(OAc)_2$ (28 mg, 0.12 mmol), 1,3-bis-(diphenylphosphino)propane (77 mg, 0.19 mmol) in 6 mL of DMA). This reaction mixture was then allowed to stir at 120 °C for 48 h followed by removal of the DMA using a vacuum oven. The residue was then treated with hot ethanol and filtered. Recrystallization in EtOH gave **9** (120 mg, 39%) as off-white crystals. ^{1}H NMR (400 MHz, $CDCl_3$, δ): 3.69 (broad s, 4H), 4.22 (broad s, 4H), 7.27−7.41 (m, 8H), 7.57−7.62 (m, 8H), 7.76 (d, J = 8.0 Hz, 2H), 8.06 (s, 2H). ^{13}C{^{1}H} NMR (100 MHz, $CDCl_3$, δ): 61.7 (broad, 4C), 92.9 (2C), 122.5 (2C), 126.7 (2C), 126.9 (2C), 126.9 (4C), 128.1 (2C), 128.4 (2C), 129.0 (4C), 130.1 (2C), 132.5 (4C), 133.5 (2C), 137.3 (2C), 139.2 (2C). HRMS (MALDI-TOF) m/z calculated for $C_{34}H_{28}O_4$ [M]$^+$, 500.1988; found, 500.1984.

General Procedure for Mallory Bis-Photocyclization-Dehydrogenation. A solution of the bisstyrylphenanthrene substrate (0.5 mM), I_2 (2.2 mol equiv), and propylene oxide (50 mol equiv) in toluene was heated or cooled to the desired temperature and subsequently irradiated overnight in a Pyrex vessel with a 600 W medium pressure mercury vapor lamp. The reaction mixture was allowed to cool or warm to room temperature and was washed with sodium thiosulfate three times and DI water three times and finally with brine. The toluene was removed, and the sample was dried in a vacuum oven overnight prior to NMR analysis. No precipitate was visible in any of the NMR samples.

5,6-Bis-ethyleneketal-naphtho[2,1-*b*]pentahelicene (10d). A solution of **9** (100 mL, 0.5 mM), I_2 (1.1 mM), and propylene oxide (25 mM) in toluene was placed in an ice-bath. The reaction mixture temperature was maintained at 0 °C and irradiated for 13 h with a 600 W medium pressure mercury vapor lamp. The organic reaction product was washed with sodium thiosulfate three times and water three times and dried over $MgSO_4$. The solvent was removed at reduced pressure, and the crude product was purified by silica gel chromatography (1:4 EtOAc:hexanes) to give **10d** as a colorless solid. ^{1}H NMR (600 MHz, $CDCl_3$, δ): 3.40 (d, J = 11.1 Hz, 1H), 3.53 (dd, J = 2.3 Hz, 11.1 Hz, 1H), 3.79 (td, J = 2.5 Hz, 12.3 Hz, 1H), 3.94 (dd, J = 2.1 Hz, 12.0 Hz, 1H), 4.11 (d, J = 7.3 Hz, 2H), 4.60−4.68 (m, 2H), 7.0 (t, J = 7.7 Hz, 1H), 7.34 (d, J = 8.9 Hz, 1H), 7.42 (t, J = 7.0 Hz, 1H), 7.61 (t, J = 7.2 Hz, 1H), 7.63 (d, 8.7 Hz, 1H), 7.69 (t, J = 7.7, 1H), 7.73 (d, J = 8.7 Hz, 1H), 7.80 (d, J = 8.8 Hz, 1H), 7.85 (d, J = 8.4 Hz, 1H), 7.87 (s, 2H), 8.14 (s, 1H), 8.36 (d, J = 8.6 Hz, 1H), 8.81 (d, J = 8.3 Hz, 1H), 9.09 (s, 1H). ^{13}C{^{1}H} NMR (100 MHz, $CDCl_3$, δ): 59.1 (1C), 59.4 (1C), 63.5 (1C), 63.9 (1C), 92.7 (1C), 93.2 (1C), 120.4 (1C), 123.0 (1C), 123.6 (1C), 124.1 (1C), 126.5 (1C), 126.7 (1C), 126.8 (1C), 126.9 (1C), 126.9 (1C), 127.7 (1C), 127.8 (1C), 128.0 (1C), 128.0 (1C), 128.6 (1C), 129.5 (1C), 129.5 (1C), 129.6 (1C), 129.6 (1C), 130.3 (1C), 130.4 (1C), 130.8 (1C), 131.9 (1C), 132.3 (1C), 132.4 (1C), 132.7 (1C), 133.1 (1C), 133.3 (1C), 134.8 (1C). HRMS (MALDI-TOF) m/z calculated for $C_{34}H_{24}O_4$ [M]$^+$, 496.1675; found, 496.1680.

Naphtho[2,3-*l*]heptahelicene (11c). To a solution of 9,10-[7]helicenequinone (6.2 mg, 15.2 μmol), *O*-xylenebis-(triphenylphosphonium bromide) (21.5 mg, 27.4 μmol), and tetra-*n*-butylammonium perchlorate (3 mg, 8.8 μmol) in CH_2Cl_2 (2 mL), 2 mL of freshly prepared LiOH solution (0.5 M, 7 mg of Li metal in 2 mL of water) was added. The two-phase mixture was sonicated for 90 min. The reaction product was extracted with toluene and washed with water. The crude product was purified by silica gel chromatography (100% hexanes) to give **11c** (1.3 mg, 18%) as a pale yellow solid. ^{1}H NMR (600 MHz, $CDCl_3$, δ): 6.43 (ddd, J = 1.3 Hz, 6.8 Hz, 8.3 Hz, 2H), 6.89 (d, J = 8.5, 2H), 6.93 (ddd, J = 1.1 Hz, 6.8 Hz, 7.87 Hz, 2H), 7.27 (d, J = 7.9 Hz, 2H), 7.40 (d, J = 8.5 Hz, 2H), 7.62−7.63 (m, 2H), 7.67 (d, J = 8.5 Hz, 2H), 8.07 (d, J = 8.4 Hz, 2H), 8.19−8.21 (m, 2H), 8.95 (d, J = 8.6 Hz, 2H), 9.27 (s, 2H). ^{13}C{^{1}H} NMR (100 MHz, $CDCl_3$, δ): 121.2 (2C), 122.3 (2C), 123.6 (2C), 125.0 (2C), 125.4 (2C), 125.4 (2C), 126.0 (2C), 126.1 (2C), 126.5 (2C), 127.2 (2C), 127.9 (2C), 128.3 (2C), 129.0 (2C), 129.6 (2C), 129.7 (2C), 129.8 (2C), 131.7 (2C), 131.8 (2C), 132.4 (2C). HRMS (MALDI-TOF) m/z calculated for $C_{38}H_{22}$ [M]$^+$, 478.1722; found, 478.1717.

Dibenzo[*c*,*m*]-naphtho[2,3,*h*]pentaphene (12c). A solution of crude **8** (100 mg, 0.21 mmol), I_2 (116 mg, 0.46 mmol), and propylene oxide (725 μL, 103.6 mmol) in toluene (420 mL) was heated up to 95 °C in a 500 mL Pyrex flask. Once the target temperature was reached, the sample was irradiated with a 600 W medium pressure mercury vapor lamp for 20 h. The reaction solution was allowed to cool to room temperature and then washed with sodium thiosulfate to remove unreacted iodine and subsequently washed with water. The reaction product was passed through a silica gel plug using toluene to give **12c** (57.2 mg, 58%) as a yellow solid. ^{1}H NMR (400 MHz, $CDCl_3$, δ): 7.61 (dd, J = 7.8 Hz, 7.8 Hz, 2H), 7.69 (dd, J = 7.7 Hz, 7.7 Hz, 2H), 7.72−7.73 (m, 2H), 7.87 (d, J = 7.6 HZ, 2H), 8.36−8.37 (m, 2H), 8.59−8.66 (m, 4H), 8.77 (d, J = 8.5 Hz, 2H), 8.82 (d, J = 8.82 Hz, 2H), 9.67 (dd, J = 3 Hz, 8.7 Hz, 2H), 9.78 (d, J = 5.6 Hz, 2H). HRMS (MALDI-TOF) m/z calculated for $C_{38}H_{22}$ [M]$^+$, 478.1722; found, 478.1714.

7,8-Bis-ethyleneketal-dibenzo[*c*,*m*]pentaphene (12d). A solution of **9** (100 mL, 0.5 mM), I_2 (1.1 mM), and propylene oxide (25 mM) in toluene was prepared in a 250 mL Pyrex glass pressure vessel. The reaction mixture was heated to 157 °C and subsequently irradiated for 18 h with a 600 W medium pressure mercury vapor lamp. The reaction mixture was washed with sodium thiosulfate three times and water three times and dried over $MgSO_4$. The solvent was removed at reduced pressure, and the reaction product was purified by recrystallization in toluene/EtOH to afford **12d** as a colorless solid. ^{1}H NMR (600 MHz, $CDCl_3$, δ): 3.84 (broad s, 4H), 4.41 (broad s, 4H), 7.64 (ddd, J = 1.0 Hz, 7.1 Hz, 7.9 Hz, 2H), 7.70 (ddd, J = 1.3 Hz, 7.1 Hz, 8.2 Hz, 2H), 7.82 (d, J = 8.8 Hz, 2H), 7.89 (d, J = 8.8 Hz, 2H), 7.92 (d, 7.8 Hz, 2H), 8.62 (s, 2H), 8.82 (d, 8.3 Hz, 2H), 9.14 (s, 2H). ^{13}C{^{1}H} NMR (100 MHz, $CDCl_3$, δ): 93.3 (2C), 121.1 (2C), 123.1 (2C), 124.2 (2C), 126.8 (2C), 126.9 (2C), 127.0 (2C), 128.3 (2C), 128.7 (2C), 130.4 (2C), 130.6 (2C), 131.3 (2C), 131.3 (2C), 132.2 (2C), 133.2 (2C). HRMS (MALDI-TOF) m/z calculated for $C_{34}H_{24}O_4$ [M]$^+$, 496.1675; found, 496.1676.

3,6-Bis-styrylphenanthrenequinone. A mixture of 3,6-dibromophenanthrenequinone (100 mg, 0.27 mmol), tetra-*n*-butylammonium bromide (35 mg, 0.11 mmol), and K_2CO_3 (189 mg, 1.37 mmol) in 1.5 mL of DMA was stirred and heated up to 120 °C under nitrogen for 48 h. When 60 °C was reached, the reaction mixture was charged with styrene (85 mg, 0.82 mmol). When 90 °C was reached, a prepared palladium catalyst solution was added dropwise ($Pd(OAc)_2$ (0.6 mg, 2.7 μmol), 1,3-bis(diphenylphosphino)propane (1.4 mg, 3.28 μmol) in 1.5 mL of DMA). The DMA was removed using a vacuum oven. The reaction product was purified by silica gel chromatography (3:2 hexanes:ethyl acetate) to afford 3,6-bis-styrylphenanthrenequinone (20.8 mg, 19%) as a red film. ^{1}H NMR (400 MHz, $CDCl_3$, δ): 7.26 (d, J = 7.8 Hz, 16.0 Hz, 2H), 7.34−7.45 (m, 8H), 7.62 (d, J = 7.7 Hz, 4H), 7.67 (d, 8 Hz, 2H), 8.15 (s, 2H), 8.23 (d, J = 8.1 Hz, 2H).

5,6-Dimethoxy-2-pentahelicenecarboxaldehyde (15b). A solution of **7** (100 mL, 0.5 mM), I_2 (2.2 mol equiv), and propylene oxide (50 mol equiv) in toluene was irradiated overnight with a 600 W medium pressure mercury vapor lamp. The organic reaction product was washed with sodium thiosulfate three times and water three times and dried over $MgSO_4$. The toluene was filtered and

DOI: 10.1021/acs.joc.8b02671
J. Org. Chem. 2019, 84, 817−830

removed under reduced pressure, and the crude reaction product was purified by silica gel chromatography (1% EtOAc in hexanes) to afford **15b** as a yellow solid. ^{1}H NMR (600 MHz, $CDCl_3$, δ): 4.20 (s, 3H), 4.21 (s, 3H), 7.24 (ddd, J = 1.4 Hz, 7.0 Hz, 8.3 Hz, 1H), 7.53 (ddd, J = 1.0 Hz, 7.0 Hz, 7.9 Hz, 1H), 7.91 (d, J = 8.5 Hz, 1H), 7.96–7.99 (m, 3H), 8.02 (dd, J = 1.5 Hz, 8.6 Hz, 1H), 8.31 (d, 8.5 Hz, 1H), 8.39 (d, 8.4 Hz, 1H), 8.40 (d, 8.5 Hz, 1H), 8.92 (s, 1H), 9.72 (s, 1H). ^{13}C{^{1}H} NMR (100 MHz, $CDCl_3$, δ): 61.5 (1C), 61.5 (1C), 121.1 (1C), 122.9 (1C), 123.5 (1C), 124.9 (1C), 125.8 (1C), 126.5 (1C), 126.9 (1C), 127.0 (1C), 128.1 (1C), 128.3 (1C), 128.4 (1C), 128.6 (1C), 128.7 (1C), 130.0 (1C), 130.7 (1C), 132.0 (1C), 132.3 (1C), 132.7 (1C), 133.1 (1C), 135.9 (1C), 144.4 (1C), 146.9 (1C), 192.6 (1C). HRMS (MALDI-TOF) m/z calculated for $C_{25}H_{18}O_3$ $[M]^+$, 366.1256; found, 366.1257.

Naphtho[2,3-*f*]-2-pentahelicenecarboxylaldehyde (15c). A solution of **8** (100 mL, 0.5 mM), I_2 (2.2 mol equiv), and propylene oxide (50 mol equiv) in toluene was placed in an ice-bath and irradiated for 14 h with a 600 W medium pressure mercury vapor lamp. The organic reaction product was washed with sodium thiosulfate three times and water three times and dried over $MgSO_4$. The toluene was filtered and removed under reduced pressure, and the reaction product was purified by slilica gel chromatography (1% EtOAc in hexanes) to afford **15c** as a yellow solid. ^{1}H NMR (600 MHz, $CDCl_3$, δ): 7.21 (ddd, J = 1.3 Hz, 6.8 Hz, 8.3 Hz, 1H), 7.51 (ddd, J = 1.0 Hz, 6.8 Hz, 7.9 Hz, 1H), 7.63–7.65 (m, 2H), 7.89 (d, 8.5 Hz, 1H), 7.92 (d, 8.6 Hz, 1H), 7.95 (dd, J = 1.0 Hz, 8.0 Hz, 1H), 8.05 (d, 8.3 Hz, 1H), 8.06 (dd, J = 1.6 Hz, 8.3 Hz, 1H), 8.14–8.19 (m, 2H), 8.38 (d, 8.4 Hz, 1H), 8.73 (d, 1.2 Hz, 1H), 8.74 (d, 8.6 Hz, 1H), 8.80 (d, 8.3 Hz, 1H), 9.07 (s, 1H), 9.19 (s, 1H), 9.73 (s, 1H). ^{13}C{^{1}H} NMR (100 MHz, $CDCl_3$, δ): 121.5 (1C), 123.1 (1C), 123.4 (1C), 124.8 (1C), 124.9 (1C), 125.2 (1C), 126.2 (1C), 126.6 (1C), 126.8 (1C), 126.9 (1C), 126.9 (1C), 127.5 (1C), 128.0 (1C), 128.2 (1C), 128.3 (1C), 128.4 (1C), 128.4 (1C), 128.7 (1C), 129.0 (1C), 129.3 (1C), 130.5 (1C), 131.2 (1C), 131.4 (1C), 132.2 (1C), 132.9 (1C), 133.1 (1C), 133.2 (1C), 133.4 (1C), 134.9 (1C), 135.6 (1C), 192.1 (1C). HRMS (MALDI-TOF) m/z calculated for $C_{31}H_{18}O$ $[M]^+$, 406.1358; found, 406.1358.

■ ASSOCIATED CONTENT

Supporting Information

The Supporting Information is available free of charge on the ACS Publications website at DOI: 10.1021/acs.joc.8b02671.

cif report (CIF)

computational details (Cartesian coordinates, zero point energy, thermochemical data) (PDF)

1D and 2D proton and carbon NMR data, comparator NMR plots (PDF)

■ AUTHOR INFORMATION

Corresponding Author

*E-mail: clennane@uwyo.edu.

ORCID

E. L. Clennan: 0000-0002-9851-1129

Notes

The authors declare no competing financial interest.

■ ACKNOWLEDGMENTS

This material is based upon work supported by the National Science Foundation under CHE-1147542 and CHE-1762161. In memory of Frank Mallory 1933–2017.

■ REFERENCES

(1) Smakula, A. The photochemical transformation of *trans*-stilbene. *Z. Phys. Chem.* **1934**, *B25*, 90–98.

(2) Parker, C. O.; Spoerri, P. E. Photochemical Conversion of Stilbene to Phenanthrene. *Nature* **1950**, *166*, 603.

(3) Mallory, F. B.; Wood, C. S.; Gordon, J. T.; Lindquist, L. C.; Savitz, M. L. Photochemistry of Stilbenes. I. *J. Am. Chem. Soc.* **1962**, *84*, 4361–4362.

(4) Moore, W. M.; Morgan, D. D.; Stermitz, F. R. The Photochemical Conversion of Stilbene to Phenanthrene. The Nature of the Intermediate. *J. Am. Chem. Soc.* **1963**, *85*, 829–830.

(5) Doyle, T. D.; Filipescu, N.; Benson, W. R.; Banes, D. Photocyclization of a, a' -Diethyl-4,4'-stilbenediol. Isolation of a Stable Tautomer of the Elusive Dihydrophenanthrenes. *J. Am. Chem. Soc.* **1970**, *92*, 6371–6372.

(6) Doyle, T. D.; Benson, W. R.; Filipescu, N. Photocyclization of Diethylstilbestrol. Isolation of a Stable, Self-Trapping Dihydrophenanthrene Intermediate. *J. Am. Chem. Soc.* **1976**, *98*, 3262–3267.

(7) Cuppen, J. H. M.; Laarhoven, W. H. Photodehydrocyclizations of Stilbene-Like Compounds. VI. Chemical Evidence of an Excited State Mechanism. *J. Am. Chem. Soc.* **1972**, *94*, 5914–5915.

(8) Irie, M.; Fukaminato, T.; Matsuda, K.; Kobatake, S. Photochromism of Diarylethene Molecules and Crystals: Memories, Switches, and Actuators. *Chem. Rev.* **2014**, *114*, 12174–12277.

(9) Flammang-Barbieux, M.; Nasielski, J.; Martin, R. H. Synthesis of heptahelicene (1) benzo [c] phenanthro [4, 3-g]phenanthrene. *Tetrahedron Lett.* **1967**, *8*, 743–744.

(10) Martin, R. H. The Helicenes. *Angew. Chem., Int. Ed. Engl.* **1974**, *13*, 649–660.

(11) Gingras, M. One hundred years of helicene chemistry. Part 3: applications and properties of carbohelicenes. *Chem. Soc. Rev.* **2013**, *42*, 1051–1095.

(12) Gingras, M. One hundred years of helicene chemistry. Part 1: non-stereoselective syntheses of carbohelicenes. *Chem. Soc. Rev.* **2013**, *42*, 968–1006.

(13) Gingras, M.; Felix, G.; Peresutti, R. One hundred years of helicene chemistry. Part 2: stereoselective synthesis and chiral separations of carbohelicenes. *Chem. Soc. Rev.* **2013**, *42*, 1007–1050.

(14) Laarhoven, W. H. Photochemical cyclizations and intramolecular cycloadditions of conjugated aryl olefins. Part I. Photocyclization with dehydrogenation. *Rec. Trav. Chim.-J. R. Neth. Chem.* **1983**, *102*, 185–204.

(15) Mallory, F. B.; Mallory, C. W. Photocyclization of Stilbenes and Related Molecules. In *Organic Reactions*; Dauben, W. G., Ed.; John Wiley & Sons: New York, 1984; Vol. *30*, pp 1–456.

(16) Laarhoven, W. H. Photocyclizations and Intramolecular Photocycloadditions of Conjugated Arylolefins and Related Compounds. *Org. Photochem.* **1989**, *10*, 163–308.

(17) Meier, H. The Photochemistry of Stilbenoid Compounds and Their Role in Materials Technology. *Angew. Chem., Int. Ed. Engl.* **1992**, *31*, 1399–1420.

(18) Tominaga, Y.; Castle, R. N. Photocyclization of aryl- and heteroaryl-2-propenoic acid derivatives. Synthesis of polycyclic heterocycles. *J. Heterocycl. Chem.* **1996**, *33*, 523–538.

(19) Hagen, S.; Hopf, H. Modern routes to extended aromatic compounds. In *Topics in Current Chemistry*; de Meijere, A., Ed.; Carbon Rich Compounds I; Springer-Verlag: Berlin, Heidelberg, 1998; Vol. *196*, pp 45–89.

(20) Liu, L.; Yang, B.; Katz, T. J.; Poindexter, M. K. Improved methodology for photocyclization reactions. *J. Org. Chem.* **1991**, *56*, 3769–3775.

(21) Sudhakar, A.; Katz, T. J.; Yang, B. W. Synthesis of a helical metallocene oligomer. *J. Am. Chem. Soc.* **1986**, *108*, 2790–2791.

(22) Sudhakar, A.; Katz, T. J. Directive effect of bromine on stilbene photocyclizations. an improved synthesis of [7]helicene. *Tetrahedron Lett.* **1986**, *27*, 2231–2234.

(23) Liu, L.; Katz, T. J. Bromine auxiliaries in photosyntheses of [5]helicenes. *Tetrahedron Lett.* **1991**, *32*, 6831–6834.

(24) Finnie, A. A.; Hill, R. A. The synthesis of 1,5,7,10-tetraoxygenated 3-methylphenanthrenes. *J. Chem. Res., Synop.* **1987**, 78–79.

(25) Mallory, F. B.; Rudolph, M. J.; Oh, S. M. Photochemistry of stilbenes. 8. Eliminative photocyclization of o-methoxystilbenes. *J. Org. Chem.* **1989**, *54*, 4619−4626.
(26) Li, Z.; Twieg, R. J. Photocyclodehydrofluorination. *Chem. - Eur. J.* **2015**, *21*, 15534−15539.
(27) Morin, J.-F.; Daigle, M.; Desroches, M. Photochemical and Direct C-H Arylation Routes toward Carbon Nanomaterials. In *Synthetic Methods for Conjugated Polymers and Carbon Materials*, 1st ed.; Leclerc, M., Morin, J.-F., Eds.; Wiley-VCH Verlag GmbH & Co. KGaA: 2017; pp 229−253.
(28) Ern, J.; Bens, A. T.; Martin, H. D.; Mukamel, S.; Schmid, D.; Tretiak, S.; Tsiper, E.; Kryschi, C. Reaction dynamics of photochromic dithienylethene derivatives. *Chem. Phys.* **1999**, *246*, 115−125.
(29) Bens, A. T.; Ern, J.; Kuldova, K.; Trommsdorff, H. P.; Kryschi, C. Reaction and excited state relaxation dynamics of photochromic dithienylethene derivatives. *J. Lumin.* **2001**, *94*−*95*, 51−54.
(30) Hania, P. R.; Telesca, R.; Lucas, L. N.; Pugzlys, A.; van Esch, J.; Feringa, B. L.; Snijders, J. G.; Duppen, K. An Optical and Theoretical Investigation of the Ultrafast Dynamics of a Bisthienylethene-Based Photochromic Switch. *J. Phys. Chem. A* **2002**, *106*, 8498−8507.
(31) Bearpark, M. J.; Bernardi, F.; Clifford, S.; Olivucci, M.; Robb, M. A.; Vreven, T. Cooperating Rings in cis-Stilbene Lead to an S0/S1 Conical Intersection. *J. Phys. Chem. A* **1997**, *101*, 3841−3847.
(32) Dou, Y.; Allen, R. E. Dynamics of the photocyclization of *cis*-stilbene to dihydrophenanthrene. *J. Mod. Opt.* **2004**, *51*, 2485−2491.
(33) Harabuchi, Y.; Keipert, K.; Zahariev, F.; Taketsugu, T.; Gordon, M. S. Dynamics Simulations with Spin-Flip Time-Dependent Density Functional Theory: Photoisomerization and Photocyclization Mechanisms of cis-Stilbene in $\pi\pi^*$ States. *J. Phys. Chem. A* **2014**, *118*, 11987−11998.
(34) Ioffe, I. N.; Granovsky, A. A. Photoisomerization of Stilbene: The Detailed XMCQDPT2 Treatment. *J. Chem. Theory Comput.* **2013**, *9*, 4973−4990.
(35) Dulić, D.; Kudernac, T.; Pužys, A.; Feringa, B. L.; vanWees, B. J. Temperature Gating of the Ring-Opening Process in Diarylethene Molecular Switches. *Adv. Mater.* **2007**, *19*, 2898−2902.
(36) Sumi, T.; Takagi, Y.; Yagi, A.; Morimoto, M.; Irie, M. Photoirradiation wavelength dependence of cycloreversion quantum yields of diarylethenes. *Chem. Commun.* **2014**, *50*, 3928−3930.
(37) Martin, R. H.; Flammang-Barbieux, M.; Cosyn, J. P.; Gelbcke, M. 1-Synthesis of octa- and nonahelicenes. 2-New syntheses of hexa- and heptahelicenes. 3-Optical rotation and O.R.D. of heptahelicene. *Tetrahedron Lett.* **1968**, *9*, 3507−3510.
(38) Laarhoven, W. H.; Cuppen, T. H. J. H. M.; Nivard, R. J. F. Photodehydrocyclizations in stilbene-like compounds—III: Effect of steric factors. *Tetrahedron* **1970**, *26*, 4865−4881.
(39) Laarhoven, W. H.; Cuppen, T. J. H. M.; Nivard, R. J. F. Photodehydrocyclizations in stilbene-like compounds. *Rec. Trav. Chim.* **1968**, *87*, 687−698.
(40) Burkitt, F. H.; Coulson, C. A.; Longuet-Higgins, H. C. Free valence in unsaturated hydrocarbons. *Trans. Faraday Soc.* **1951**, *47*, 553−564.
(41) Yuan, Z.; Xiao, Y.; Qian, X. A design concept of planar conjugated ladder oligomers of perylene bisimides and efficient synthetic strategy via regioselective photocyclization. *Chem. Commun.* **2010**, *46*, 2772−2774.
(42) Shi, S.; Nawaz, K. S.; Zaman, M. K.; Sun, Z. Advances in Enantioselective C-H Activation/Mizoroki-Heck Reaction and Suzuki Reaction. *Catalysts* **2018**, *8*, 90.
(43) Talele, H. R.; Chaudhary, A. R.; Patel, P. R.; Bedekar, A. V. Expeditious synthesis of helicenes using an improved protocol of photocyclodehydration of stilbenes. *ARKIVOC* **2011**, *ix*, 15−37.
(44) Ben Hassine, B.; Gorsane, M.; Pecher, J.; Martin, R. H. Diastereoselective NaBH4 Reductions of (dl) a-Keto Esters. *Bull. Soc. Chim. Belg.* **1985**, *94*, 597−603.
(45) Grandbois, A.; Collins, S. K. Enantioselective Synthesis of [7]Helicene: Dramatic Effects of Olefin Additives and Aromatic Solvents in Asymmetric Olefin Metathesis. *Chem. - Eur. J.* **2008**, *14*, 9323−9329.
(46) Sapir, M.; Vander Donckt, E. Intersystem Crossing in the Helicenes. *Chem. Phys. Lett.* **1975**, *36*, 108−110.
(47) Birks, J. B.; Birch, D. J. S.; Cordemans, E.; Vander Donckt, E. Fluorescence of the higher helicenes. *Chem. Phys. Lett.* **1976**, *43*, 33−36.
(48) Grellmann, K.-H.; Hentzschel, P.; Wismontski-Knittel, T.; Fischer, E. The photophysics and photochemistry of pentahelicene. *J. Photochem.* **1979**, *11*, 197−213.
(49) Wilkinson, F.; Helman, W. P.; Ross, A. B. *J. Phys. Chem. Ref. Data* **1993**, *22*, 113−262.
(50) Gorman, A. A.; Gould, I. R.; Hamblett, I. Time-Resolved Study of the Solvent and Temperature Dependence of Singlet Oxygen (1Δg) Reactivity toward Enol Ethers: Reactivity Parameters Typical of Rapid Reversible Exciplex Formation. *J. Am. Chem. Soc.* **1982**, *104*, 7098−7104.
(51) Clar, E. *The Aromatic Sextet*; John Wiley & Sons: London, 1972.
(52) Hemelsoet, K.; De Vleeschouwer, F.; Van Speybroeck, V.; De Proft, F.; Geerlings, P.; Waroquier, M. Validation of DFT-Based Methods for Predicting Qualitative Thermochemistry of Large Polyaromatics. *ChemPhysChem* **2011**, *12*, 1100−1108.
(53) Wismontski-Knittel, T.; Kaganowitch, M.; Seger, G.; Fischer, E. The reversible photochemistry of 1,2-di-(2-naphthyl)cyclopentene. *Rec. Trav. Chim.* **1979**, *98*, 114−117.
(54) Muszkat, K. A. The 4a, 4b-Dihydrophenanthrenes. *Topics Curr. Chem.* **1980**, *88*, 89−143.
(55) Hammond, G. S.; Saltiel, J.; Lamola, A. A.; Turro, N. J.; Bradshaw, J. S.; Cowan, D. O.; Counsell, R. C.; Vogt, V.; Dalton, C. Mechanisms of Photochemical Reactions in Solution. XXII.1 Photochemical cis-trans Isomerization. *J. Am. Chem. Soc.* **1964**, *86*, 3197−3217.
(56) Klan, P.; Wirz, J. *Photochemistry of Organic Compounds. From Concepts to Practice*; John Wiley & Sons Ltd.: U.K., 2009.
(57) Saltiel, J.; Charlton, J. L. *Rearrangements in Ground and Excited States*; Academic Press: New York, 1980; Vols. *42*/*43*.
(58) Fleming, G. R. Subpicosecond Spectroscopy. *Annu. Rev. Phys. Chem.* **1986**, *37*, 81−104.

DOI: 10.1021/acs.joc.8b02671
J. Org. Chem. 2019, 84, 817−830